





Andreev reflections in black phosphorus based normal-superconducting junctions modulated by linearly polarized light

Shu-Gang Chen , Xiangru Kong , Bin-Yuan Zhang, and Wei-Jiang Gong ^{*}
College of Sciences, Northeastern University, Shenyang 110819, China

 (Received 7 December 2023; revised 23 February 2024; accepted 27 March 2024; published 9 April 2024)

We perform investigations about the Andreev reflections (ARs) in normal-superconducting (NS) junctions based on the few-layer black phosphorus, by considering the irradiation of the linearly polarized off-resonant light. Following the analysis on the band structures, we propose the types of ARs in such NS junctions. Specifically, it has been found that when the incident energy E is less than the Fermi energy E_F , the intraband retro AR occurs, and otherwise the interband specular AR is achieved. A forbidden region of ARs is formed between the retro AR and the specular AR since the band gap leads to a momentum-filtering feature. By using the linearly polarized off-resonant light along y direction, we are allowed to modify the size of this forbidden region. On the other hand, when the normal direction of the NS-junction interface is changed from parallel to perpendicular, by using the linearly polarized off-resonant light along x direction, the retro and specular ARs can be transformed into each other, resulting in an anisotropic differential conductance, which is a unique observable signature for AR in the experiment.

DOI: [10.1103/PhysRevB.109.165418](https://doi.org/10.1103/PhysRevB.109.165418)

I. INTRODUCTION

Following the discovery of graphene, two-dimensional (2D) materials have become a research hotspot in solid-state physics both theoretically and experimentally due to abundant physics connotations and potential application values. In 2D materials, more quantum degrees of freedom, such as spin, pseudospin, energy valley, and layer, further attract the research interest of scientist, which also expands their application possibility in the fields of condensed-matter physics and nanoelectronics [1–4]. Accordingly, various 2D materials have been predicted and achieved in experiments [5–8], including compounds and simple substances. Regarding simple substances, it has been shown that black phosphorus (BP) is one typical 2D material, which is formed by the overlapping splicing of multilayer phosphorus atoms [9,10]. Its crystal structure exhibits a layered structure similar to graphene, with each layer composed of hexagonal phosphorus atoms and adjacent layers stacked by weak van der Waals forces [11]. This structure allows BP to display many unique physics properties, e.g., tunable band gap [12], highly anisotropic optical [13,14] and thermal properties [15,16], and very high mobility [17].

Due to the unique properties of BP, novel quantum transport phenomena have also received extensive attention. Recently, Long *et al.* have investigated the quantum transport properties of high-mobility electrons and holes in atomically thin BP ambipolar devices [18]. In addition, Choi *et al.* proved that the pseudospin structure plays an important role in the tunneling properties of BP junctions and found the

Klein tunneling phenomenon [19]. Some researches have also observed the anomalous Klein tunneling in BP junctions [20,21]. Meanwhile, interesting transport phenomena have been observed in monolayer phosphorene-based p - n junctions, including the negative reflection and anti-super-Klein tunneling [22].

It should be noticed that AR is one kind of important transport phenomena [23]. Unlike single-electron transport, the ARs of BP heterojunctions will be more interesting. Moreover, according to the study of Beenakker [24], AR has its new physical picture in graphene-like 2D materials, and they first predicted the specular AR in graphene-based normal-superconducting (NS) junctions, with the electron and hole from the conduction and valence bands, respectively, in which only the velocity component perpendicular to the interface is inverted [25–28]. This indeed enriches the pictures of the AR in the 2D materials, such as graphene and borophene [29–32]. Following the investigation of the transport properties of monolayer phosphorene heterojunctions in experiments [33–35] and theories [36,37], attention has been drawn to the AR and Josephson effects [38,39]. One can thus notice that it is necessary to study the ARs in the BP-based NS (BP-NS) junctions, since BP is a typical phosphorene. According to existing studies, both the experimental and theoretical aspects have made sufficient preparations for the description of the ARs by designing the BP-NS junctions [40–44].

In the present paper, we would like to pay attention to the AR behaviors in the BP-NS junctions, to clarify the retro and specular ARs determined by the electronic band structure of BP. Meanwhile, it is known that during the past years, the light field has been applied to the study of 2D materials, such as graphene [45–48], silicene [49,50], borophene [51], and phosphorus [52], to modulate their properties determined

^{*}gwj@mail.neu.edu.cn

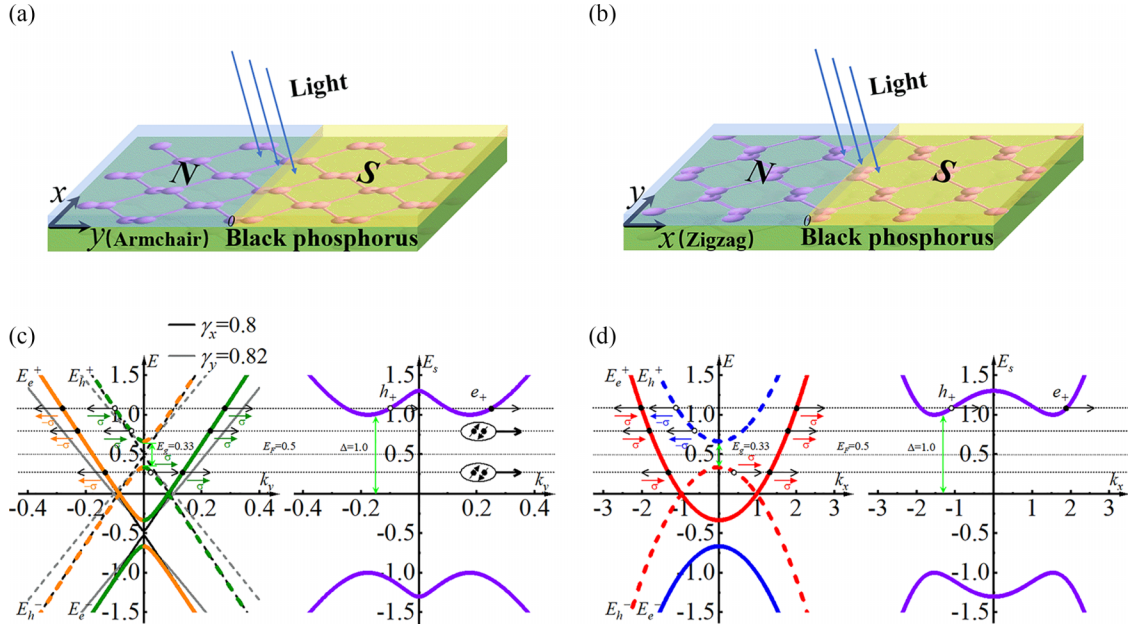


FIG. 1. Schematic diagram for the BP-NS junctions irradiated by the linearly polarized off-resonant light for (a) the armchair direction and (b) the zigzag direction. Dispersion relations for electrons and holes in the BP and superconductor for (c) the armchair direction and (d) the zigzag direction. In (c) and (d), black and gray lines indicate the presence of the light field with the linearly polarized light along the y and x directions, respectively, while colored lines denote the absence of the light field. Colored arrows (σ) represent pseudospin directions.

by the band structures. In BP, the pseudospin-selective light-induced band renormalization has also been demonstrated [53]. This means that the light field is able to modify the AR in the BP-NS junctions. Therefore, we aim to discuss the ARs modulated by the linearly polarized off-resonant light in the BP-NS junctions [see Figs. 1(a) and 1(b)]. By using the Floquet theory of periodically driven quantum systems [47,48], we obtain the effective Hamiltonians of the linearly polarized off-resonant light modulation along the y and x directions, respectively. After calculation, we confirm that the types of ARs on the surface of the BP-NS junctions are the retro AR ($E < E_F$) or the specular AR ($E > E_F$) in the armchair direction, and the existence of the band gap will cause the forbidden region of ARs between the retro and specular ARs. Due to the influence of pseudospin, the AR in the zigzag direction is suppressed. Interestingly, when the interface orientation angle is equal to zero in the BP-NS junctions, the band gap is reduced by the linearly polarized off-resonant light along the x direction. This effect can be utilized to adjust the size of the forbidden region of ARs. If the interface orientation angle θ of the BP-NS junctions is varied from 0° to 90° , the tilting degree of the energy band is changed due to the linearly polarized off-resonant light along the x direction. The retro AR will gradually evolve into the specular AR in the case of $E < E_F$, and the maximal differential conductance appears at $\theta \neq 0^\circ$. Alternatively if $E > E_F$, the retro AR will gradually evolve into the specular AR, and then specular AR gradually evolves into the retro AR again, with the maximal differential conductance at $\theta = 0^\circ$. These results indicate that in the armchair direction of the BP-NS junctions, the AR-related transport properties are strongly anisotropic

due to the adjustment of the band structures by the linearly polarized off-resonant light.

II. THEORY

According to the previous studies, the low-energy effective Hamiltonian of few-layer BP can be written as [54,55]

$$H_\eta(\mathbf{k}) = \eta \left[\left(\frac{E_g}{2} + \frac{\hbar^2 k_x^2}{2m^*} \right) \sigma_x + \hbar v_y k_y \sigma_y \right], \quad (1)$$

where $\eta = +(-)$ represents electron (hole) index, $\mathbf{k} = (k_x, k_y)$ is the wavevector along zigzag and armchair directions, respectively, and $m^* = 1.42m_e$ is the effective mass along the zigzag direction (m_e is the free electron mass). E_g is the band gap, whose magnitude varies from 0.35 eV in bulk to 1.73 eV in the monolayer BP structure. In addition, $v_y = 5.6 \times 10^5$ m/s is the velocity along the armchair direction. $\sigma_{x(y)}$ is the $x(y)$ component of the Pauli matrix.

We firstly consider the polarization of the linearly polarized off-resonant light along y direction with the vector potential $A = (0, A_y)$ with $A_y = \frac{E_e}{\omega} \sin \omega t$ in which E_e is the electric field intensity and ω is the frequency of light. In such a case, the wavevector k_y in Eq. (1) will be rewritten as $k_y \rightarrow k_y - \frac{eA_y}{\hbar}$ by the canonical substitution. And then, the Hamiltonian of the light-irradiated BP is modified as

$$H_\eta^L(\mathbf{k}) = H_\eta(\mathbf{k}) + H_n, \quad (2)$$

in which $H_n = -\eta v_y e A_y \sigma_y$. According to the time-dependent Floquet Hamiltonian in the limit of the high frequency, the

effective Hamiltonian can be obtained [47,48,56], i.e.,

$$\begin{aligned}
H_\eta^{\text{eff}} &\simeq H^0 + \frac{1}{\hbar\omega} \sum_{n=1}^{\infty} \frac{1}{n} [H^{-n}, H^{+n}] \\
&+ \frac{1}{2(\hbar\omega)^2} \sum_{j=1}^{\infty} \frac{1}{j^2} \{[[H^{-j}, H^0], H^j] + \text{H.c.}\} \\
&+ \frac{1}{3(\hbar\omega)^2} \sum_{j,l=1}^{\infty} \frac{1}{jl} \{[[H^{-j}, [H^{-l}, H^{j+l}]] \\
&- [H^{-j}, [H^l, H^{-l+j}]] + \text{H.c.}\} + \mathcal{O}\left(\frac{1}{(\hbar\omega)^3}\right), \quad (3)
\end{aligned}$$

where $H^0 = H_\eta(\mathbf{k})$, $H^{\pm n} = \frac{1}{T} \int_0^T H_n e^{\pm in\omega t} dt$ ($n > 0$) are the Fourier components of the time-dependent Floquet Hamiltonian with $T = \frac{2\pi}{\omega}$ being the time period. Thus, the effective Hamiltonian above is

$$H_\eta^{\text{eff}} = \eta \left[\left(\frac{E_g}{2} + \frac{\hbar^2 k_x^2}{2m^*} \right) \lambda_x \sigma_x + \hbar v_y k_y \sigma_y \right], \quad (4)$$

in which $\lambda_x = 1 - \gamma_x$ with $\gamma_x = \left(\frac{v_y e E_c}{\hbar\omega^2}\right)^2$. On the other hand, if the polarization of the linearly polarized off-resonant light is considered to be along x direction with the vector potential $A = (A_x, 0)$ with $A_x = \frac{E_c}{\omega} \cos \omega t$, then $H_n = \eta \left(-\frac{\hbar k_x e A_x}{m^*} + \frac{(e A_x)^2}{2m^*}\right) \sigma_x$. By Eq. (3), the effective Hamiltonian is

$$H_\eta^{\text{eff}} = \eta \left[\left(\frac{E_g}{2} + \frac{\hbar^2 k_x^2}{2m^*} \right) \sigma_x + \hbar v_y^{\text{eff}} k_y \sigma_y \right], \quad (5)$$

with $v_y^{\text{eff}} = (1 - \gamma_y) v_y$ and $\gamma_y = \left(\frac{e^2 E_c^2}{8\hbar m^* \omega^2}\right)^2$. Equations (4) and (5) are similar in form, hence we would like to give an unified expression of these two effective Hamiltonians, i.e.,

$$H_\eta^{\text{eff}} = \eta \left[\left(\frac{E_g}{2} + \frac{\hbar^2 k_x^2}{2m^*} \right) \tilde{\lambda}_x \sigma_x + \hbar \tilde{v}_y k_y \sigma_y \right], \quad (6)$$

for simplifying the following derivations. Note that when linearly polarized light is applied in the y direction, $\tilde{\lambda}_x = \lambda_x$ and $\tilde{v}_y = v_y$ take their effects. Alternatively when linearly polarized light is applied in the x direction, $\tilde{v}_y = v_y^{\text{eff}}$ and $\lambda_x = 1$ display the influence.

In our BP-NS junctions, the superconducting region is achieved by the proximity effect caused by the BP structure on the surface of the s -wave superconductor. It can be understood that the Bogoliubov-de Gennes (BdG) Hamiltonian of the BP-NS junctions reads [32,57]

$$H_{\text{BdG}} = \begin{pmatrix} H_+^{\text{eff}} - E_F - U(\mathbf{r}) & \Delta(\mathbf{r}) \\ \Delta(\mathbf{r})^* & -H_-^{\text{eff}*} + E_F + U(\mathbf{r}) \end{pmatrix}, \quad (7)$$

where $U(\mathbf{r}) = U\Theta(\mathbf{r})$, $\Delta(\mathbf{r}) = \Delta\Theta(\mathbf{r})$ with the step function Θ , and E_F is the Fermi energy. In the normal region, the po-

tential and the superconductor gap are both equal to zero. On the other side, it is the superconducting region with nonzero superconductor gap Δ and large electrostatic potential U . Due to the time-reversal symmetry, we prove that $H_-^{\text{eff}*} = H_+^{\text{eff}}$.

By solving Eq. (7), we obtain the energy dispersions for electron and hole excitations in the normal region, i.e.,

$$\begin{aligned}
E_{e\pm} &= \pm \sqrt{\left[\left(\frac{E_g}{2} + \frac{\hbar^2 k_x^2}{2m^*} \right) \tilde{\lambda}_x \right]^2 + (\hbar \tilde{v}_y k_y)^2 - E_F}, \\
E_{h\pm} &= \pm \sqrt{\left[\left(\frac{E_g}{2} + \frac{\hbar^2 k_x^2}{2m^*} \right) \tilde{\lambda}_x \right]^2 + (\hbar \tilde{v}_y k_y)^2 + E_F}. \quad (8)
\end{aligned}$$

$+$ ($-$) denotes the electron in the conduction (valence) band and the hole in the valence (conduction) band. In the superconducting region, the energy dispersion is expressed as

$$\begin{aligned}
&(\sqrt{E_s^2 - \Delta^2 + U + E_F})^2 \\
&= \left[\left(\frac{E_g}{2} + \frac{\hbar^2 k_x^2}{2m^*} \right) \tilde{\lambda}_x \right]^2 + (\hbar \tilde{v}_y k_y)^2. \quad (9)
\end{aligned}$$

For the quantitative analysis, we are allowed to study in detail the amplitudes of each transport process, including the retro and specular ARs, by means of the scattering matrix method with the detailed forms of wavefunctions given in Appendix A. To begin with, we consider Ψ_{e+} to be the incident mode. It can be found that the normal reflection (NR) mode Ψ_{e-} for electron always exists regardless of the value of energy E , but the retro AR mode Ψ_{h-} for hole keeps only when $E < E_F$. If $E > E_F$, the specular AR mode Ψ_{h+} arises, replacing the retro AR mode Ψ_{h-} . Therefore the wavefunctions in the normal region can be written as follows:

$$\Psi_I(\mathbf{r}) = \begin{cases} \Psi_{e+} + r_N \Psi_{e-} + r_A \Psi_{h-}, & \text{if } E < E_F, \\ \Psi_{e+} + r_N \Psi_{e-} + r_A \Psi_{h+}, & \text{if } E > E_F. \end{cases} \quad (10)$$

where $\mathbf{r} = (y, x)$ in the armchair direction, $\mathbf{r} = (x, y)$ in the zigzag direction, r_N and r_A are the reflection amplitudes of NR and ARs, respectively. The wavefunctions in the superconducting region can be described as

$$\Psi_{\text{II}}(\mathbf{r}) = a \Psi_{sh+} + b \Psi_{se+}, \quad (11)$$

where a and b are the amplitudes of electronlike and holelike quasiparticles in the superconducting region. These coefficients, i.e., r_N , r_A , a , and b , are determined by the matching condition of the wavefunctions at the interface of the BP-NS junctions, i.e.,

$$\begin{aligned}
\Psi_I(\mathbf{r})|_{y=0^-} &= \Psi_{\text{II}}(\mathbf{r})|_{y=0^+}, & \text{armchair;} \\
\Psi_I(\mathbf{r})|_{x=0^-} &= \Psi_{\text{II}}(\mathbf{r})|_{x=0^+}, & \text{zigzag.} \quad (12)
\end{aligned}$$

By calculating Eq. (12), we obtain

$$\begin{aligned}
r_N &= \frac{(e^{i\theta_{hr}} - e^{i\theta'_{sk+}})(e^{i\theta_{k+}} - e^{i\theta_{sk+}})e^{2i\beta} - (e^{i\theta_{k+}} - e^{i\theta'_{sk+}})(e^{i\theta_{hr}} - e^{i\theta_{sk+}})}{(e^{i\theta_{hr}} - e^{i\theta_{sk+}})(e^{i\theta_{k-}} - e^{i\theta'_{sk+}}) - (e^{i\theta_{hr}} - e^{i\theta'_{sk+}})(e^{i\theta_{k-}} - e^{i\theta_{sk+}})e^{2i\beta}}, \\
r_A &= \frac{(e^{i\theta_{k-}} - e^{i\theta_{k+}})(e^{i\theta_{hr}} - e^{i\theta_{sk+}})e^{i\beta} - (e^{i\theta_{k-}} - e^{i\theta_{k+}})(e^{i\theta_{hr}} - e^{i\theta'_{sk+}})e^{i\beta}}{(e^{i\theta_{hr}} - e^{i\theta_{sk+}})(e^{i\theta_{k-}} - e^{i\theta'_{sk+}}) - (e^{i\theta_{k-}} - e^{i\theta_{sk+}})(e^{i\theta_{hr}} - e^{i\theta_{sk+}})e^{2i\beta}} \quad (13)
\end{aligned}$$

with

$$e^{i\theta_{hr}} = \begin{cases} e^{i\theta_{k-}'} & \text{if } E < E_F, \\ e^{i\theta_{k+}'} & \text{if } E > E_F. \end{cases} \quad (14)$$

Following the above results, we can calculate the NR and AR coefficients. According to the definition of the particle current density operator, we have

$$\begin{aligned} J &\equiv \frac{1}{\hbar}[(y, x), H_{\text{BdG}}] \\ &= \tau_z \otimes \left[\tilde{v}_y \sigma_y \mathbf{e}_y + \frac{\hbar k_x}{m^*} \tilde{\lambda}_x \sigma_x \mathbf{e}_x \right], \end{aligned} \quad (15)$$

where $\tau_z = \begin{pmatrix} 1 & 0 \\ 0 & -1 \end{pmatrix}$ denotes electron-hole index, and $\mathbf{e}_x, \mathbf{e}_y$ are unit vectors in x, y directions. Accordingly, the current density operator $J_y = \tau_z \otimes \tilde{v}_y \sigma_y$ decides the reflection coefficients at the armchair direction. Thus, the NR and AR coefficients R_N and R_A in the armchair direction are evaluated by

$$\begin{aligned} R_N &= \frac{|\langle \Psi_{e-} | J_y | \Psi_{e-} \rangle|}{|\langle \Psi_{e+} | J_y | \Psi_{e+} \rangle|} |r_N|^2 = \frac{|\sin \theta_{k-}|}{|\sin \theta_{k+}|} |r_N|^2, \\ R_A &= \frac{|\langle \Psi_{hr} | J_y | \Psi_{hr} \rangle|}{|\langle \Psi_{e+} | J_y | \Psi_{e+} \rangle|} |r_A|^2 = \frac{|\sin \theta_{hr}|}{|\sin \theta_{k+}|} |r_A|^2. \end{aligned} \quad (16)$$

The current density operator in the zigzag direction is $J_x = \tau_z \otimes \frac{\hbar k_x}{m^*} \tilde{\lambda}_x \sigma_x$, so R_N and R_A are given as

$$\begin{aligned} R_N &= \frac{|\langle \Psi_{e-} | J_x | \Psi_{e-} \rangle|}{|\langle \Psi_{e+} | J_x | \Psi_{e+} \rangle|} |r_N|^2 = \frac{|\cos \theta_{k-}|}{|\cos \theta_{k+}|} |r_N|^2, \\ R_A &= \frac{|\langle \Psi_{hr} | J_x | \Psi_{hr} \rangle|}{|\langle \Psi_{e+} | J_x | \Psi_{e+} \rangle|} |r_A|^2 = \frac{|\cos \theta_{hr}|}{|\cos \theta_{k+}|} |r_A|^2. \end{aligned} \quad (17)$$

Before numerical calculations, we would like to qualitatively understand the interband and intraband AR properties by observing the alignment of band and pseudospin structures. Figures 1(c) and 1(d) show the interband and intraband AR mechanisms for the BP-NS junctions along the armchair and zigzag junctions. According to the previous researches, we know that in the BP-NS junctions, the group velocity of an electron and a hole can be defined as $\mathbf{u} = \frac{1}{\hbar} \nabla_{\mathbf{k}} E$. Thus, the velocity components of electron are expressed as

$$\begin{aligned} u_{xe} &= \frac{\partial E}{\hbar \partial k_{xe}} = \frac{\frac{\hbar k_{xe}}{m^*} \tilde{\lambda}_x^2 \left(\frac{E_g}{2} + \frac{\hbar^2 k_{xe}^2}{2m^*} \right)}{\sqrt{\left[\left(\frac{E_g}{2} + \frac{\hbar^2 k_{xe}^2}{2m^*} \right) \tilde{\lambda}_x \right]^2 + (\hbar \tilde{v}_y k_{ye})^2}}, \\ u_{ye} &= \frac{\partial E}{\hbar \partial k_{ye}} = \frac{\hbar \tilde{v}_y^2 k_{ye}}{\sqrt{\left[\left(\frac{E_g}{2} + \frac{\hbar^2 k_{xe}^2}{2m^*} \right) \tilde{\lambda}_x \right]^2 + (\hbar \tilde{v}_y k_{ye})^2}}. \end{aligned} \quad (18)$$

For the hole if $E < E_F$, there will be

$$\begin{aligned} u_{xh} &= \frac{\partial E}{\hbar \partial k_{xh}} = -\frac{\frac{\hbar k_{xh}}{m^*} \tilde{\lambda}_x^2 \left(\frac{E_g}{2} + \frac{\hbar^2 k_{xh}^2}{2m^*} \right)}{\sqrt{\left[\left(\frac{E_g}{2} + \frac{\hbar^2 k_{xh}^2}{2m^*} \right) \tilde{\lambda}_x \right]^2 + (\hbar \tilde{v}_y k_{yh})^2}}, \\ u_{yh} &= \frac{\partial E}{\hbar \partial k_{yh}} = -\frac{\hbar \tilde{v}_y^2 k_{yh}}{\sqrt{\left[\left(\frac{E_g}{2} + \frac{\hbar^2 k_{xh}^2}{2m^*} \right) \tilde{\lambda}_x \right]^2 + (\hbar \tilde{v}_y k_{yh})^2}}. \end{aligned} \quad (19)$$

Instead if $E > E_F$,

$$\begin{aligned} u_{xh} &= \frac{\partial E}{\hbar \partial k_{xh}} = \frac{\frac{\hbar k_{xh}}{m^*} \tilde{\lambda}_x^2 \left(\frac{E_g}{2} + \frac{\hbar^2 k_{xh}^2}{2m^*} \right)}{\sqrt{\left[\left(\frac{E_g}{2} + \frac{\hbar^2 k_{xh}^2}{2m^*} \right) \tilde{\lambda}_x \right]^2 + (\hbar \tilde{v}_y k_{yh})^2}}, \\ u_{yh} &= \frac{\partial E}{\hbar \partial k_{yh}} = \frac{\hbar \tilde{v}_y^2 k_{yh}}{\sqrt{\left[\left(\frac{E_g}{2} + \frac{\hbar^2 k_{xh}^2}{2m^*} \right) \tilde{\lambda}_x \right]^2 + (\hbar \tilde{v}_y k_{yh})^2}}. \end{aligned} \quad (20)$$

And then, the armchair junction incident (reflection) angle of electron (hole) is

$$\varphi_{ei(hr)}^a = \arctan \frac{u_{xe(h)}}{u_{ye(h)}}, \quad (21)$$

with the counterpart in the zigzag junction being

$$\varphi_{ei(hr)}^z = \arctan \frac{u_{ye(h)}}{u_{xe(h)}}. \quad (22)$$

Here we consider the electron incident from the conduction band (E_{e+}). When $E < E_F$, the hole is reflected into the conduction band (E_{h-}), and when $E > E_F$, the hole is reflected into the valence band (E_{h+}) [see Figs. 1(c) and 1(d)]. As we know, the opposite (same) directions of transverse velocities of incident electron and reflected holes correspond to the retro AR (specular AR). Due to the same sign of u_{xe} and u_{xh} (u_{ye} and u_{yh}) in the armchair (zigzag) direction, the retro AR is presented as the intraband AR when $E < E_F$. However, the signs of u_{xe} and u_{xh} (u_{ye} and u_{yh}) in the armchair (zigzag) direction are opposite, hence the specular AR is manifested as interband when $E > E_F$. From an experimental perspective, if $\phi_{ei}^{a(z)}$ and $\phi_{hr}^{a(z)}$ have the same sign, the retro AR will come into being. On the contrary, if $\phi_{ei}^{a(z)}$ and $\phi_{hr}^{a(z)}$ have the opposite signs, the specular AR will be observed. The intraband electron-hole conversion results in the retro AR and the interband conversion is for the specular AR.

The pseudospin angle in the BP-NS junctions can be solved through Eqs. (A6) and (A14). And then,

$$\begin{aligned} \theta_{k\pm} &= \arg \left[\left(\frac{E_g}{2} + \frac{\hbar^2 k_x^2}{2m^*} \right) \tilde{\lambda}_x + i \hbar \tilde{v}_y k_{y\pm} \right], \\ \theta'_{k\pm} &= \arg \left[\left(\frac{E_g}{2} + \frac{\hbar^2 k_x^2}{2m^*} \right) \tilde{\lambda}_x + i \hbar \tilde{v}_y k'_{y\mp} \right], \end{aligned} \quad (23)$$

in the armchair direction. And in the zigzag direction, they can be expressed as

$$\begin{aligned} \theta_{k\pm} &= \arg \left[\left(\frac{E_g}{2} + \frac{\hbar^2 k_{x\pm}^2}{2m^*} \right) \tilde{\lambda}_x + i \hbar \tilde{v}_y k_y \right], \\ \theta'_{k\pm} &= \arg \left[\left(\frac{E_g}{2} + \frac{\hbar^2 (k'_{x\mp})^2}{2m^*} \right) \tilde{\lambda}_x + i \hbar \tilde{v}_y k_y \right]. \end{aligned} \quad (24)$$

Based on the above results, we are allowed to study the regulation of ARs by pseudospin in different directions. The colored arrows in Figs. 1(c) and 1(d) represent the pseudospin directions. Figure 1(c) shows that whether it is the intraband electron-hole conversion or the interband conversion, the pseudospins of incident electrons are nearly parallel to those of the reflected holes. In contrast, reflected electrons have nearly antiparallel pseudospins. As a result, we can expect the occurrence of ARs in the armchair direction. However, in the

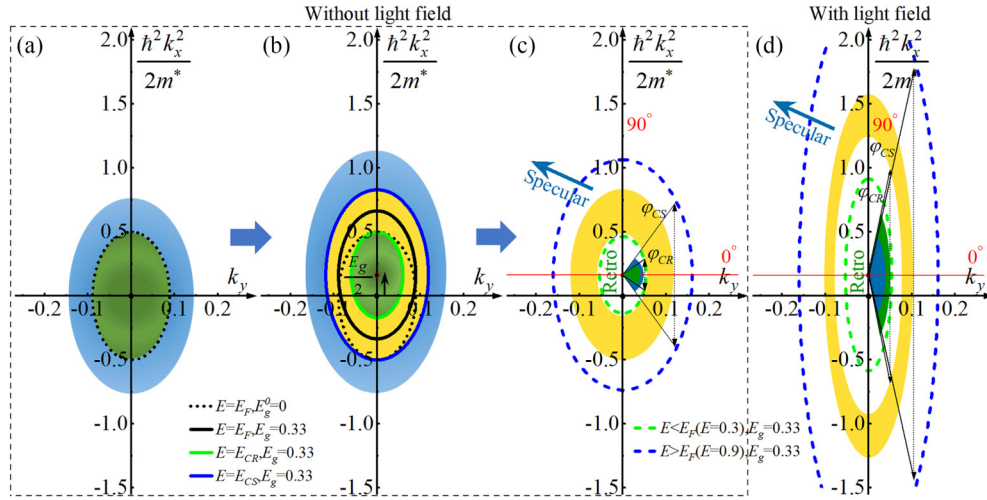


FIG. 2. [(a)–(d)] Equal-energy surfaces under different conditions. The black-dashed-lined and solid-lined circles indicate the Fermi energy of BP without and with the band gap. The upper limit of the incident energy with nonzero retro AR (E_{CR}) and the lower limit of incident energy with nonzero specular AR (E_{CS}) are represented by the solid-green line and the solid-blue line, respectively. The green-dashed line applies to cases where the incident energy is less than the Fermi energy ($E < E_F$), while the blue-dashed line applies to cases where the incident energy is greater than the Fermi energy ($E > E_F$). The yellow-ring area represents the forbidden region of ARs. The green-shaded area and blue-shaded area in (a) and (b) [(c) and (d)] indicate the ranges of incident energy [the range of incident angles of the wavevectors] where the retro and specular ARs occur, respectively. The parameters are taken as $E_F = 0.5$, (b) $E_{CR} = 0.335$, $E_{CS} = 0.665$, (d) $\gamma_x = 0.6$.

zigzag direction [see Fig. 1(d)], the pseudospin of the incident electron is parallel to that of the reflected electron, leading to the result that the incident electron is completely reflected. From the formula for pseudospin angle, i.e., $\theta_{k\pm} = \arg[(\frac{E_g}{2} + \frac{\hbar^2 k_{y\pm}^2}{2m^*})\tilde{\lambda}_x + i\hbar\tilde{v}_y k_y]$, one can observe that k_x^2 is always a positive number, so $\theta_{k+} = \theta_{k-}$. Substitute this result into Eq. (13), we can readily find $r_A = 0$. This is the fundamental reason why the AR coefficient is equal to zero in the zigzag direction. So, the pseudospin index takes its leading effect on the AR in the armchair direction, and meanwhile, it completely suppresses the AR in the zigzag direction. Due to the eliminated ARs in the zigzag direction, we will only discuss ARs in the armchair direction in the following section.

From the dispersion relations in Fig. 1(c), it can also be observed that light with polarization γ_x narrows the band gap, which in turn promotes the occurrence of ARs. Naturally, there are two questions: one is why the band gap E_g widens the forbidden region of ARs; the other is why light with polarization γ_x can promote the occurrence of ARs. In order to understand these two questions, one can focus on the example shown in Figs. 2(a)–2(d), which are the cases without and with light field, respectively. The black-dashed-lined and solid-lined circles represent the Fermi energy of BP in the absence and presence of the band gap, respectively. Here the result of zero band gap, i.e., $E_g^0 = 0$, are introduced as a reference. In Fig. 2(a), we observe that in the case of $E_g^0 = 0$, the retro AR (the green-shaded area) occurs when the incident energy is less than the Fermi energy ($E < E_F$), otherwise, the specular AR (the blue-shaded area) occurs. The band gap E_g leads to the anomalous shift of the Fermi energy E_F (the black-dashed-lined circle moves upward and varies to be the black-solid-lined circle), causing the momentum imbalance of the reflected holes, and then the forbidden region of ARs (the yellow-ring area) appears [see Fig. 2(b)]. Simply,

one may predict the range of wavevectors that allow ARs by considering the overlap of the Fermi energy of the absence and presence of the band gap. It is interesting to notice that ARs are forbidden for a certain incident energy E and incident angle of wavevector φ , namely, the wavevector filtering behavior is found. In the case of $E_{CR} \leq E \leq E_{CS}$, wavevectors $k'_{y\pm}$ become imaginary and the total NR occurs. It can be analytically found that, the upper (lower) limit of the incident energy with nonzero retro (specular) AR is

$$E_{CR(CS)} = E_F \mp \left(\frac{E_g}{2} + \frac{\hbar^2 (k \sin \varphi)^2}{2m^*} \right) (1 - \gamma_x). \quad (25)$$

While for a fixed incident energy, ARs change obviously and vanish when the incident angle of wavevector φ exceeds a critical value, i.e.,

$$\varphi_C = \begin{cases} \arcsin \sqrt{\frac{2m^*(E+E_F)}{\hbar^2 k^2 (1-\gamma_x)}} & \text{if } \gamma_x \neq 1, \\ 90^\circ & \text{if } \gamma_x = 1. \end{cases} \quad (26)$$

If $E < E_F$, there will be $\varphi_{CR} = \varphi_C$ (the green-shaded area), otherwise $\varphi_{CS} = \varphi_C$ (the blue-shaded area) [see Figs. 2(c) and 2(d)]. By comparing Figs. 2(c) and 2(d), we find that the existence of the light field narrows the forbidden region of ARs and enlarges the range of the incident angle of wavevector with nonzero retro (specular) AR. Using Eqs. (25) and (26), we can also see that an increase in γ_x leads to a decrease in $E_{CR(CS)}$, an increase in φ_C , and a reduction in the forbidden region of ARs. On the other hand, the light with polarization γ_x will change the tilting degree of the energy band [see Fig. 1(c)] and induce some intricate transport phenomena, which will be discussed in detail in Sec. III B.

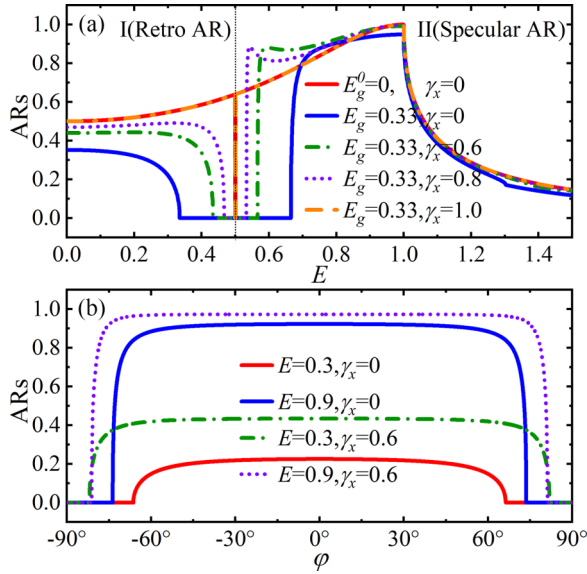


FIG. 3. (a) The retro and specular ARs coefficients vs the incident energy E with $\varphi = 0^\circ$. (b) The retro and specular ARs coefficients as functions of the incident angle of wavevector φ .

III. NUMERICAL RESULTS AND DISCUSSIONS

In this section, we proceed to investigate the ARs and conductance spectra of the BP-NS junctions. Before calculation, we would like to define an angle θ , which describes the intersection angle of the normal of the BP-NS junction interface with the y bias [see Fig. 5(a) below], and then perform calculations by considering the cases of $\theta = 0^\circ$ and $\theta \neq 0^\circ$, respectively. In addition, we set $\hbar = 1.0$, $m^* = 1.42$, $v_y = 5.6$, $E_g = 0.33$, $E_F = 0.5$, $U = 0.5$, and $\Delta = 1.0$ unless other statements, and suppose the energy unit to be eV in the context, which is ignored in the following for convenience. In the following discussion, we also use the result of zero band gap (i.e., $E_g^0 = 0$) as a reference, to better demonstrate the effect of linearly polarized light on BP with its fixed band gap $E_g = 0.33$.

A. ARs for $\theta = 0^\circ$

As shown in Sec. II, the light with polarization along the y direction can narrow the band gap of BP [see Fig. 1(c)], so it can be believed that an interesting quantum transport phenomenon could occur when interface orientation angle is equal to zero ($\theta = 0^\circ$) and linearly polarized light is applied in the y direction. In such a case, there will be $\tilde{\lambda}_x = \lambda_x = 1 - \gamma_x$ and $\tilde{v}_y = v_y$ [see Fig. 1(a)]. In Fig. 3, we show the retro and specular ARs coefficients vs the incident energy E . Based on the qualitative analysis presented in Sec. II, it is evident that the retro AR occurs in case I ($0 < E < 0.5$), and the specular AR comes up in case II where $E > 0.5$. Firstly, in the absence of light field with $E_g^0 = 0$, the retro AR changes smoothly in the low-energy region and then goes up as energy E increases. When $E > 0.5$, the specular AR increases with the increment of E . However, due to the tunneling of electrons in the superconducting interface, the specular AR experiences a sharp decline $E > \Delta$. When the band gap $E_g = 0.33$, ARs

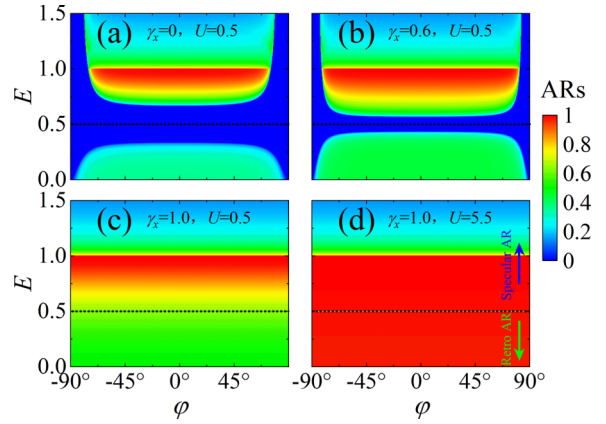


FIG. 4. Three-dimensional spectra of the retro and specular ARs as functions of E and φ . The black-dashed line ($E = E_F$) represents the boundary between the two ARs.

are forbidden for incident energy $E_F - \frac{E_g}{2}(1 - \gamma_x) < E < E_F + \frac{E_g}{2}(1 - \gamma_x)$, which means there is a forbidden region of incident energy. Then, the retro and specular AR coefficients as functions of the incident angle of wavevector φ are shown in Fig. 3(b). We find that the forbidden region of the incident angle of the wavevector of the retro AR ($E = 0.3$) is larger than that of the specular AR ($E = 0.9$), and the coefficient of the retro AR is smaller than that of the specular AR. Next, in the presence of a light field, $\gamma_x \neq 0$, it is interesting to notice that the forbidden region of incident energy and forbidden region of incident angle of the wavevector of ARs become smaller as the increase of the light with polarization γ_x . In short, γ_x is beneficial for the occurrence of ARs.

Combining with Figs. 3(a) and 3(b), we observe that the light with polarization γ_x will narrow the forbidden region of ARs and enlarges the range of incident angles of wavevector φ of ARs. To more clearly observe the impact of γ_x and U on ARs, in Figs. 4(a)–4(d) we display the three-dimensional spectra of the retro and specular ARs as functions of E and φ . Figures 4(a) and 4(b) illustrate the existence of both retro and specular ARs, with a forbidden region between them. The boundary of this forbidden region can be approximately given by the relationship $E_{CR(CS)}$. The ARs change significantly and disappear when the incident energy E exceeds a critical value, for a fixed incident angle. Similarly, for a fixed incident energy, the ARs change significantly and vanish when the incident angle of wave vector φ exceeds a critical value φ_C . Figure 4(c) shows that the blue forbidden region of ARs shrinks with increasing γ_x and then disappears at $\gamma_x = 1.0$. Additionally, we can also observe that the retro AR is greatly improved as the increase of γ_x , while the specular AR is less impacted by changes in γ_x . Upon comparing Figs. 4(c) and 4(d), we observe perfect retro AR when $E < E_F$ and perfect specular AR when $E_F < E < \Delta$ for all incidence angles of the wavevector by increasing the electrostatic potential U .

B. ARs for $\theta \neq 0^\circ$

The theory in Sec. II also shows that linearly polarized light in the x direction is capable of altering the tilting degree of the energy band [see Fig. 1(c)]. Thus, it is necessary to consider

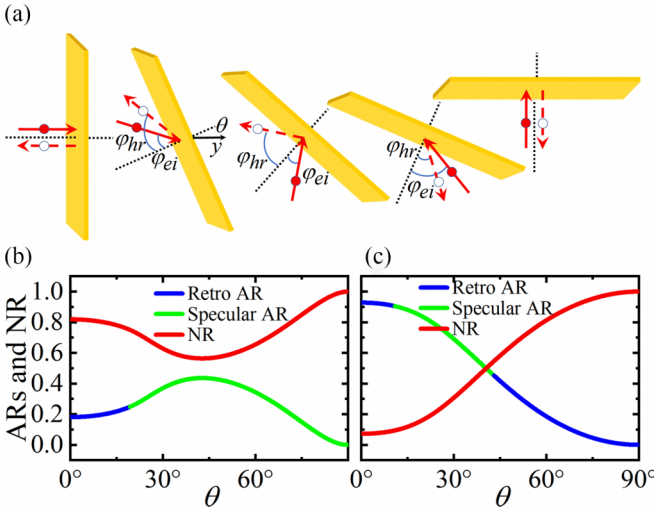


FIG. 5. (a) Schematic diagrams of ARs when changing the BP-NS interface orientation angle θ . The coefficients of ARs and NR vs θ for (b) $\tilde{E} = 0.3/E_0$, $\gamma_y = 0.92$, and (c) $\tilde{E} = 0.9/E_0$, $\gamma_y = 0.92$.

the possibility of the anisotropic transport phenomenon resulting from the nonzero orientation angle ($\theta \neq 0^\circ$) of the BP-NS interface and the light with polarization along x direction. And then, the relevant parameters are taken as $\tilde{v}_y = v_y^{\text{eff}} = (1 - \gamma_y)v_y$ and $\lambda_x = 1$ [see Fig. 5(a)]. For convenience, we use dimensionless units: the momentum scale $P_0 = 2m^*v_y^{\text{eff}}$, the energy scale $E_0 = \frac{p_0^2}{2m^*}$, and the length scale $l_0 = \hbar/P_0$. In doing so, one can define the dimensionless quantities as $\tilde{E}_F = E_F/E_0$, $\tilde{\Delta} = \Delta/E_0$, $\tilde{U} = U/E_0$, $\tilde{E} = E/E_0$, $\tilde{E}_g = E_g/E_0$, $\tilde{k}_y = \hbar k_y/P_0$, $\tilde{k}_x = \hbar k_x/P_0$, and $\tilde{x}(\tilde{y}) = x(y)/l_0$. The relationship between the wavevector components in the $\tilde{y} - \tilde{x}$ and $\tilde{y}' - \tilde{x}'$ coordinate systems through the transformation between the vector components are [58,59]

$$\begin{aligned}\tilde{k}_y &= \tilde{k}_{y'} \cos \theta - \tilde{k}_{x'} \sin \theta, \\ \tilde{k}_x &= \tilde{k}_{y'} \sin \theta + \tilde{k}_{x'} \cos \theta.\end{aligned}\quad (27)$$

Then, the details of related calculation of AR and NR coefficients are given in Appendix B. We obtain the velocity components of the electron and hole at a nonzero orientation angle using Eqs. (18)–(20), i.e.,

$$\begin{aligned}u_{xe} &= \frac{\partial \tilde{E}}{\hbar \partial \tilde{k}_{xe}} = \frac{2(\frac{\tilde{E}_g}{2} + \tilde{k}_{xe}^2)\tilde{k}_{xe} \cos \theta - \tilde{k}_{ye} \sin \theta}{\sqrt{(\frac{\tilde{E}_g}{2} + \tilde{k}_{xe}^2)^2 + \tilde{k}_{ye}^2}}, \\ u_{ye} &= \frac{\partial \tilde{E}}{\hbar \partial \tilde{k}_{ye}} = \frac{2(\frac{\tilde{E}_g}{2} + \tilde{k}_{xe}^2)\tilde{k}_{xe} \sin \theta + \tilde{k}_{ye} \cos \theta}{\sqrt{(\frac{\tilde{E}_g}{2} + \tilde{k}_{xe}^2)^2 + \tilde{k}_{ye}^2}}.\end{aligned}\quad (28)$$

If $\tilde{E} < \tilde{E}_F$,

$$\begin{aligned}u_{xh} &= \frac{\partial \tilde{E}}{\hbar \partial \tilde{k}_{xh}} = -\frac{2(\frac{\tilde{E}_g}{2} + \tilde{k}_{xh}^2)\tilde{k}_{xh} \cos \theta - \tilde{k}_{yh} \sin \theta}{\sqrt{(\frac{\tilde{E}_g}{2} + \tilde{k}_{xh}^2)^2 + \tilde{k}_{yh}^2}}, \\ u_{yh} &= \frac{\partial \tilde{E}}{\hbar \partial \tilde{k}_{yh}} = -\frac{2(\frac{\tilde{E}_g}{2} + \tilde{k}_{xh}^2)\tilde{k}_{xh} \sin \theta + \tilde{k}_{yh} \cos \theta}{\sqrt{(\frac{\tilde{E}_g}{2} + \tilde{k}_{xh}^2)^2 + \tilde{k}_{yh}^2}}.\end{aligned}\quad (29)$$

If $\tilde{E} > \tilde{E}_F$,

$$\begin{aligned}u_{xh} &= \frac{\partial \tilde{E}}{\hbar \partial \tilde{k}_{xh}} = \frac{2(\frac{\tilde{E}_g}{2} + \tilde{k}_{xh}^2)\tilde{k}_{xh} \cos \theta - \tilde{k}_{yh} \sin \theta}{\sqrt{(\frac{\tilde{E}_g}{2} + \tilde{k}_{xh}^2)^2 + \tilde{k}_{yh}^2}}, \\ u_{yh} &= \frac{\partial \tilde{E}}{\hbar \partial \tilde{k}_{yh}} = \frac{2(\frac{\tilde{E}_g}{2} + \tilde{k}_{xh}^2)\tilde{k}_{xh} \sin \theta + \tilde{k}_{yh} \cos \theta}{\sqrt{(\frac{\tilde{E}_g}{2} + \tilde{k}_{xh}^2)^2 + \tilde{k}_{yh}^2}}.\end{aligned}\quad (30)$$

Figure 5(a) corresponds to the schematic diagram of the evolutions of the retro and specular ARs when the BP-NS interface orientation angle θ is varied. The incident (reflection) angle of electron (hole) is defined as $\varphi_{ei(hr)} = \arctan \frac{u_{xe(h)}}{u_{ye(h)}}$. More interestingly, when the orientation angle increases to the critical angle $\theta_{c1} = \arcsin \sqrt{\frac{1}{2} - \frac{\tilde{E}_g}{\tilde{k}_{y+}'}}$, the retro AR is converted into the specular AR. When the orientation angle continues to increase to the critical angle $\theta_{c2} = \arcsin \sqrt{\frac{1}{2} - \frac{\tilde{E}_g}{\tilde{k}_{y-}'}}$, the specular AR is converted into the retro AR again. The reason is that when the interface orientation angle θ changes, the direction of the incident angle of the electron and the reflection angle of the hole will change to be the same or opposite, which will lead to the conversion between retro and specular ARs. The coefficients of AR and NR vs θ are shown in Figs. 5(b) and 5(c). First, when $\tilde{E} < \tilde{E}_F$, with the increase of the orientation angle θ , the retro AR coefficient goes up. Then, the retro AR is converted to the specular AR at the critical angle $\theta_{c1} = 19.29^\circ$. With further increase of the orientation angle θ from $\theta = \theta_{c1}$, the specular AR coefficient is first increased and then decreased gradually. Next, when $\tilde{E} > \tilde{E}_F$, due to the increase of the electron reflection coefficient, the AR coefficient gradually decreases. When the orientation angle θ increases to $\theta_{c1} = 10.81^\circ$, the specular AR replaces the retro AR. As the orientation angle θ continues to increase to $\theta_{c2} = 42.98^\circ$, the retro AR in turn replaces the specular AR.

Considering $\tilde{E} < \tilde{E}_F$, we present the θ -dependent u_{xei} , u_{xhr} , φ_{ei} , and φ_{hr} in the different γ_y in Fig. 6. As a matter of fact, the signs of u_{yei} and u_{yhr} will be opposite naturally and the signs of u_{xei} and u_{xhr} will decide the types of ARs. In Fig. 6(a), with $\gamma_y = 0.82$, only the retro AR occurs since the signs of u_{xei} and u_{xhr} are always opposite, while the signs of φ_{ei} and φ_{hr} are the same. Figures 6(b) and 6(c) demonstrate that with the change of the light γ_y , u_{xhr} remains positive and unchanged, while u_{xei} changes from negative to positive. This results in a transformation from the retro AR (where the signs of φ_{ei} and φ_{hr} are the same) to the specular AR (where the signs of φ_{ei} and φ_{hr} are opposite). In Fig. 6(d), when γ_y reaches 0.97, only the retro AR can be seen. However, unlike Fig. 6(a), u_{xei} is positive while u_{xhr} is negative. As a result, the incident angle of the electron φ_{ei} and the reflection angle of the hole φ_{hr} become positive and move to the other side of the normal line [see Fig. 5(a)].

On the other hand, we present the θ -dependent u_{xei} , u_{xhr} , φ_{ei} , and φ_{hr} in the different γ_y when $\tilde{E} > \tilde{E}_F$. The numerical results are shown in Fig. 7. Firstly, it can be found that in the case of $\gamma_y = 0.82$ and $\gamma_y = 0.87$, Figs. 7(a) and 7(b) show the same results as Figs. 6(a) and 6(b). In comparison with Figs. 7(b) and 6(b), one can see that Fig. 7(b) has a retro-specular AR conversion when the orientation angle is small.

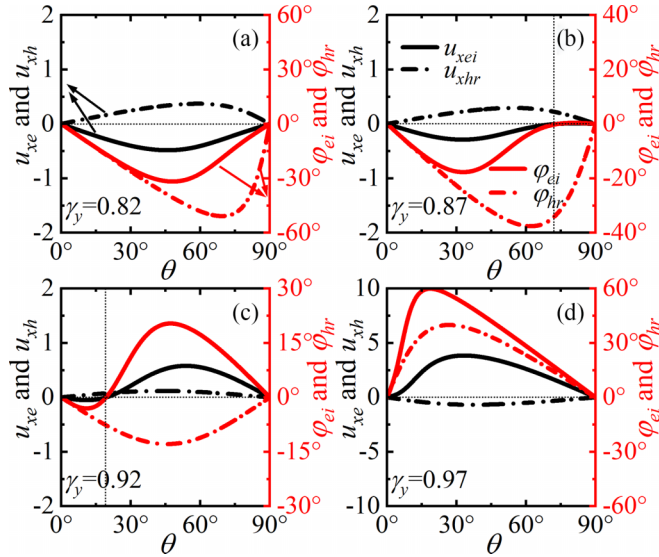


FIG. 6. Transverse velocities of incident electron (reflected hole), the incident angle of electron, and the reflection angle of hole as functions of orientation angle θ in $\tilde{E} = 0.3/E_0$ and the different γ_y .

In Fig. 7(c) where $\gamma_y = 0.92$, the retro AR is transformed into the specular AR, and then the specular AR is transformed into the retro AR again. Interestingly, we can clearly understand that the first AR transition occurs when u_{xei} changes from negative to positive and ϕ_{ei} changes from negative to positive. The second AR shift happens when u_{xhr} goes from positive to negative and ϕ_{hr} goes from negative to positive. When γ_y is equal to 0.97 [see Fig. 7(d)], the behavior is the same as that of Fig. 6(d), and only the retro AR occurs. All the analysis above clearly shows the spatial anisotropy of ARs.

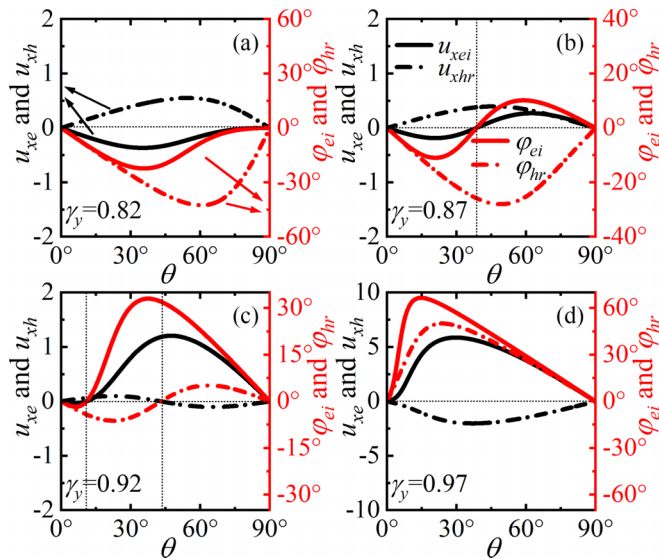


FIG. 7. Transverse velocities of incident electron (reflected hole), the incident angle of electron, and the reflection angle of hole as functions of orientation angle θ in $\tilde{E} = 0.9/E_0$ and the different γ_y .

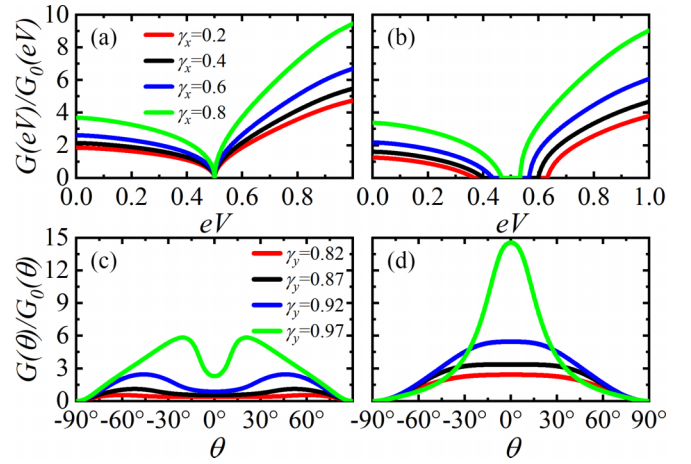


FIG. 8. [(a),(b)] Conductance $G(eV)$ vs the bias eV with the interface orientation angle $\theta = 0^\circ$ and the different γ_x . [(c),(d)] The differential conductance $G(\theta)$ as a function of θ with different γ_y . The parameters are (a) $E_g^0 = 0$, (b) $E_g = 0.33$, (c) $\tilde{eV} = 0.3/\tilde{E}_0$, (d) $\tilde{eV} = 0.9/\tilde{E}_0$.

C. Conductance spectra

After the analysis of ARs and NR above, we would like to study the properties of differential conductance, since it is a measurable quantity in the experiment. Thus, in accordance with the Blonder-Tinkham-Klapwijk (BTK) formula, the differential conductance along the y direction can be written as [60]

$$G(eV) = \frac{2e^2W}{\hbar} \int \frac{dk_x}{2\pi} [1 - R_N(eV, k_x, \theta) + R_A(eV, k_x, \theta)], \quad (31)$$

where W is the width along x direction of the BP-NS junctions. It is convenient to normalize the conductance by $G_0(eV) = \frac{2e^2W}{\pi\hbar} \sqrt{\frac{2m^*}{\hbar^2} \frac{(eV + E_F - \frac{E_g}{2})}{1 - \gamma_x}}$. Then through Eq. (31), we can rewrite the partial differential conductance of $\theta \neq 0$, i.e.,

$$G(\theta) = G_0(\theta) \int d\tilde{k}_x [1 - R_N(\tilde{eV}, \tilde{k}_x, \theta) + R_A(\tilde{eV}, \tilde{k}_x, \theta)], \quad (32)$$

with $G_0(\theta) = \frac{2e^2W}{\pi\hbar} \sqrt{\frac{-f + \sqrt{f^2 - 4g \cos^4 \theta}}{2 \cos^4 \theta}}$. Here, $f = \tilde{E}_g \cos^2 \theta + \sin^2 \theta$ and $g = (\frac{\tilde{E}_g}{2})^2 - (\tilde{eV} + \tilde{E}_F)^2$.

Figures 8(a) and 8(b) show the conductance $G(eV)$ vs the bias for the angle $\theta = 0^\circ$ with different γ_x in the cases of $E_g^0 = 0$ and $E_g = 0.33$, respectively. In Fig. 8(a) where $E_g^0 = 0$, it can be observed that the magnitude of differential conductance $G(eV)$ increases as γ_x is improved. Besides, the conductance vanishes when $eV = E_F$. This is because the differential conductance is dominated by the retro and specular ARs. $eV = E_F$ can act as the boundary between the retro and specular ARs. In Fig. 8(b) with $E_g = 0.33$, the differential conductance has the same trend as the result in Fig. 8(a). Comparing the results in Fig. 8(a) with Fig. 8(b), one can see that the increase of the band gap leads to the emergence of the conductance forbidden region due to the

absence of AR in the regimes of $E_F - \left(\frac{E_g}{2} + \frac{\hbar^2 k_{x\pm}^2}{2m^*}\right)(1 - \gamma_x) < eV < E_F + \left(\frac{E_g}{2} + \frac{\hbar^2 k_{x\pm}^2}{2m^*}\right)(1 + \gamma_x)$. Figures 8(c) and 8(d) show the spectra of conductance $G(\theta)$ as a function of θ with different γ_y in the cases of $\tilde{e}V < \tilde{E}_F$ and $\tilde{e}V > \tilde{E}_F$. In Fig. 8(c) with $\tilde{e}V = 0.3/\tilde{E}_0$, it is shown that the value of differential conductance $G(\theta)$ is enhanced as γ_y increases and the maximum differential conductance occurs at a nonzero orientation angle. On the other hand, in the case of $\tilde{e}V = 0.9/\tilde{E}_0$, the change trends of Fig. 8(d) when the orientation angle is small with γ_y are consistent with those of Fig. 8(c). When the orientation angle is large, the conductance value of $\gamma_y = 0.97$ is less than any conductance value of $\gamma_y < 0.97$. Regarding the results in Figs. 8(c) and 8(d) for the same value of γ_y , we find that the value of differential conductance in Fig. 8(d) is larger than that in Fig. 8(c) except $\gamma_y = 0.97$ when the orientation angle is large. Unlike Fig. 8(c), the maximal differential conductance arises at a zero orientation angle. The reason for this huge difference is that when $\tilde{e}V < \tilde{E}_F$, a large number of electrons are reflected, which weakens the formation of AR and leads to a decrease in conductance $G(\theta)$. On the contrary, when $\tilde{e}V > \tilde{E}_F$, a small amount of electrons are reflected, which enhances the formation of AR and makes its conductance $G(\theta)$ reach the peak. This result is consistent with what we discussed in Sec. III A for the interface orientation angle $\theta = 0^\circ$ [see Fig. 3(b)]. Obviously, due to the light-tunable anisotropic band structure of BP, the differential conductance on the BP-NS junctions is strongly anisotropic.

IV. SUMMARY

In summary, we have investigated the AR behaviors in the BP-NS junctions, which are irradiated by the linearly polarized off-resonant light, and then determined the types of the ARs: when the incident energy $E < E_F$ (Fermi energy), the electrons are incident from the conduction band and reflected to the conduction band, it is the retro AR of intraband conversion. When $E > E_F$, the electrons are reflected the valence band, it is the specular AR of interband conversion. Owing to the suppression of the ARs in the zigzag direction by the pseudospin, the above ARs can only occur in the armchair direction. Furthermore, we have found that the forbidden region of ARs between the retro and specular ARs can be adjusted by the linearly polarized off-resonant light along y direction, and perfect AR can be tuned by electrostatic potential U . On the other hand, by varying the BP-NS interface orientation angle θ and applying linearly polarized off-resonant light along the x direction, it is possible to undergo two conversions between the retro and specular ARs. Finally, we have also discussed the conductance through the BP-NS junctions and found two interesting conductance behaviors. One is that when the interface orientation angle $\theta = 0^\circ$, the conductance is strongly suppressed when $E = E_F$, and the other is the conductance strong anisotropy when interface orientation angle $\theta \neq 0^\circ$. It can be believed that our paper gives an alternative and flexible method to tune the ARs of BP.

ACKNOWLEDGMENTS

This work was financially supported by the Liaoning Revitalization Talents Program (Grant No. XLYC1907033), the

Natural Science Foundation of Liaoning province (Grant No. 2023-MS-072), the National Natural Science Foundation of China (Grant No. 11905027), and the Fundamental Research Funds for the Central Universities (Grants No. N2209005 and No. N2205015).

APPENDIX A: WAVEFUNCTIONS OF THE NORMAL AND SUPERCONDUCTING REGIONS

In this Appendix, we give wavefunctions of the normal and superconducting regions in the BP-NS junctions, by considering the armchair and zigzag directions.

The BdG equation on the normal side is

$$\begin{pmatrix} H_+^{\text{eff}} - E_F & 0 \\ 0 & E_F - H_+^{\text{eff}} \end{pmatrix} \begin{pmatrix} u_e \\ v_h \end{pmatrix} = E \begin{pmatrix} u_e \\ u_h \end{pmatrix}, \quad (\text{A1})$$

in which u_e and v_h are the electron and hole wavefunctions. At a given incident energy E and the incident angle of wavevector φ in the armchair direction,

$$k_x = k \sin \varphi, \quad (\text{A2})$$

where

$$k = \begin{cases} \sqrt{\frac{-c}{b}} & \text{if } \varphi = 0^\circ, \\ \sqrt{\frac{-b + \sqrt{b^2 - 4ac}}{2a}} & \text{if } \varphi \neq 0^\circ, \end{cases} \quad (\text{A3})$$

with

$$\begin{aligned} a &= \frac{\hbar^4 \tilde{\lambda}_x^2}{4m^{*2}} \sin^4 \varphi, \\ b &= \frac{\hbar^2 \tilde{\lambda}_x^2 E_g}{2m^*} \sin^2 \varphi + \hbar^2 \tilde{v}_y^2 \cos^2 \varphi, \\ c &= \frac{\tilde{\lambda}_x^2 E_g^2}{4} - (E + E_F)^2. \end{aligned} \quad (\text{A4})$$

The eigenstates are

$$\begin{aligned} \Psi_{e\pm}(y, x) &= \begin{pmatrix} 1 \\ e^{i\theta_{k\pm}} \\ 0 \\ 0 \end{pmatrix} e^{i(k_{y\pm}y + k_x x)}, \\ \Psi_{h+}(y, x) &= \begin{pmatrix} 0 \\ 0 \\ 1 \\ e^{i\theta'_{k+}} \end{pmatrix} e^{i(k'_{y-}y + k_x x)}, \quad \text{if } E > E_F, \\ \Psi_{h-}(y, x) &= \begin{pmatrix} 0 \\ 0 \\ 1 \\ e^{i\theta'_{k-}} \end{pmatrix} e^{i(k'_{y+}y + k_x x)}, \quad \text{if } E < E_F, \end{aligned} \quad (\text{A5})$$

in which

$$\begin{aligned} e^{i\theta_{k\pm}} &= \frac{\left(\frac{E_g}{2} + \frac{\hbar^2 k_x^2}{2m^*}\right) \tilde{\lambda}_x + i\hbar \tilde{v}_y k_{y\pm}}{\sqrt{\left[\left(\frac{E_g}{2} + \frac{\hbar^2 k_x^2}{2m^*}\right) \tilde{\lambda}_x\right]^2 + (\hbar \tilde{v}_y k_{y\pm})^2}}, \\ e^{i\theta'_{k\pm}} &= \mp \frac{\left(\frac{E_g}{2} + \frac{\hbar^2 k_x^2}{2m^*}\right) \tilde{\lambda}_x + i\hbar \tilde{v}_y k'_{y\mp}}{\sqrt{\left[\left(\frac{E_g}{2} + \frac{\hbar^2 k_x^2}{2m^*}\right) \tilde{\lambda}_x\right]^2 + (\hbar \tilde{v}_y k'_{y\mp})^2}}, \end{aligned}$$

$$k_{y\pm} = \pm \frac{1}{\hbar\tilde{v}_y} \sqrt{(E + E_F)^2 - \left[\left(\frac{E_g}{2} + \frac{\hbar^2 k_x^2}{2m^*} \right) \tilde{\lambda}_x \right]^2},$$

$$k'_{y\pm} = \pm \frac{1}{\hbar\tilde{v}_y} \sqrt{(E - E_F)^2 - \left[\left(\frac{E_g}{2} + \frac{\hbar^2 k_x^2}{2m^*} \right) \tilde{\lambda}_x \right]^2}. \quad (\text{A6})$$

The wavefunctions $\Psi_{e\pm}$ ($\Psi_{h\pm}$) are the eigenstates for electrons (holes) in the conduction band E_{e+} (E_{h-}) and valence band E_{e-} (E_{h+}).

On the other hand, the BdG equation in the superconducting region is represented as

$$\begin{pmatrix} H_+^{\text{eff}} - U\sigma_0 - E_F & \Delta_0\sigma_0 \\ \Delta_0\sigma_0 & E_F - H_+^{\text{eff}} + U\sigma_0 \end{pmatrix} \begin{pmatrix} u_e \\ v_h \end{pmatrix} = E \begin{pmatrix} u_e \\ v_h \end{pmatrix}. \quad (\text{A7})$$

The outgoing wavefunctions in the superconducting region are

$$\Psi_{sh+}(y, x) = \begin{pmatrix} e^{-i\beta} \\ e^{i\theta'_{sk+}} e^{-i\beta} \\ 1 \\ e^{i\theta'_{sk+}} \end{pmatrix} e^{i(k'_{sy+}y + k_x x)},$$

$$\Psi_{se+}(y, x) = \begin{pmatrix} e^{i\beta} \\ e^{i\theta_{sk+}} e^{i\beta} \\ 1 \\ e^{i\theta_{sk+}} \end{pmatrix} e^{i(k_{sy+}y + k_x x)}, \quad (\text{A8})$$

where

$$\beta = \begin{cases} \arccos(E/\Delta) & \text{if } E < \Delta, \\ -i \operatorname{arccosh}(E/\Delta) & \text{if } E > \Delta, \end{cases}$$

$$e^{i\theta'_{sk+}} = \frac{\left(\frac{E_g}{2} + \frac{\hbar^2 k_x^2}{2m^*} \right) \tilde{\lambda}_x + i\hbar\tilde{v}_y k'_{sy+}}{\sqrt{\left[\left(\frac{E_g}{2} + \frac{\hbar^2 k_x^2}{2m^*} \right) \tilde{\lambda}_x \right]^2 + (\hbar\tilde{v}_y k'_{sy+})^2}},$$

$$e^{i\theta_{sk+}} = \frac{\left(\frac{E_g}{2} + \frac{\hbar^2 k_x^2}{2m^*} \right) \tilde{\lambda}_x + i\hbar\tilde{v}_y k_{sy+}}{\sqrt{\left[\left(\frac{E_g}{2} + \frac{\hbar^2 k_x^2}{2m^*} \right) \tilde{\lambda}_x \right]^2 + (\hbar\tilde{v}_y k_{sy+})^2}}, \quad (\text{A9})$$

$$k'_{sy+} = -\sqrt{(i\tau_1 - \tau_2)^2 - \left[\left(\frac{E_g}{2} + \frac{\hbar^2 k_x^2}{2m^*} \right) \frac{\tilde{\lambda}_x}{\hbar\tilde{v}_y} \right]^2},$$

$$k_{sy+} = \sqrt{(i\tau_1 + \tau_2)^2 - \left[\left(\frac{E_g}{2} + \frac{\hbar^2 k_x^2}{2m^*} \right) \frac{\tilde{\lambda}_x}{\hbar\tilde{v}_y} \right]^2},$$

with $\tau_1 = \frac{\Delta \sin \beta}{\hbar\tilde{v}_y}$ and $\tau_2 = \frac{U + E_F}{\hbar\tilde{v}_y}$. The eigenstates Ψ_{sh+} , Ψ_{se+} are the superpositions of electron and hole excitations in the superconducting region. The above is the wavefunctions in the armchair direction.

Following the above derivations, we can also give the wavefunctions of the normal and superconducting regions in the zigzag direction. Firstly, the BdG equation of the normal

region can be given in Eq. (A1), by a single set of parameters (φ, E) , where

$$k_y = k \cos \varphi, \quad (\text{A10})$$

with

$$k = \begin{cases} \sqrt{\frac{-c}{b}} & \text{if } \varphi = 0^\circ, \\ \sqrt{\frac{-b + \sqrt{b^2 - 4ac}}{2a}} & \text{if } \varphi \neq 0^\circ, \end{cases} \quad (\text{A11})$$

and

$$a = \frac{\hbar^4 \tilde{\lambda}_x^2}{4m^{*2}} \cos^4 \varphi,$$

$$b = \frac{\hbar^2 \tilde{\lambda}_x^2 E_g}{2m^*} \cos^2 \varphi + \hbar^2 \tilde{v}_y^2 \sin^2 \varphi, \quad (\text{A12})$$

$$c = \frac{\tilde{\lambda}_x^2 E_g^2}{4} - (E + E_F)^2.$$

We can obtain four different wavefunctions,

$$\Psi_{e\pm}(x, y) = \begin{pmatrix} 1 \\ e^{i\theta_{k\pm}} \\ 0 \\ 0 \end{pmatrix} e^{i(k_{x\pm}x + k_y y)},$$

$$\Psi_{h+}(x, y) = \begin{pmatrix} 0 \\ 0 \\ 1 \\ e^{i\theta'_{k+}} \end{pmatrix} e^{i(k'_{x-}x + k_y y)}, \quad \text{if } E > E_F, \quad (\text{A13})$$

$$\Psi_{h-}(x, y) = \begin{pmatrix} 0 \\ 0 \\ 1 \\ e^{i\theta'_{k-}} \end{pmatrix} e^{i(k'_{x+}x + k_y y)}, \quad \text{if } E < E_F,$$

where

$$e^{i\theta_{k\pm}} = \frac{\left(\frac{E_g}{2} + \frac{\hbar^2 k_{x\pm}^2}{2m^*} \right) \tilde{\lambda}_x + i\hbar\tilde{v}_y k_y}{\sqrt{\left[\left(\frac{E_g}{2} + \frac{\hbar^2 k_{x\pm}^2}{2m^*} \right) \tilde{\lambda}_x \right]^2 + (\hbar\tilde{v}_y k_y)^2}},$$

$$e^{i\theta'_{k\pm}} = \mp \frac{\left(\frac{E_g}{2} + \frac{\hbar^2 (k'_{x\pm})^2}{2m^*} \right) \tilde{\lambda}_x + i\hbar\tilde{v}_y k_y}{\sqrt{\left[\left(\frac{E_g}{2} + \frac{\hbar^2 (k'_{x\pm})^2}{2m^*} \right) \tilde{\lambda}_x \right]^2 + (\hbar\tilde{v}_y k_y)^2}},$$

$$k_{x\pm} = \pm \frac{1}{\hbar} \sqrt{\frac{2m^*}{\tilde{\lambda}_x} \left(\sqrt{(E + E_F)^2 - (\hbar\tilde{v}_y k_y)^2} - \frac{E_g}{2} \tilde{\lambda}_x \right)},$$

$$k'_{x\pm} = \pm \frac{1}{\hbar} \sqrt{\frac{2m^*}{\tilde{\lambda}_x} \left(\sqrt{(E - E_F)^2 - (\hbar\tilde{v}_y k_y)^2} - \frac{E_g}{2} \tilde{\lambda}_x \right)}. \quad (\text{A14})$$

Meanwhile, one can also calculate the wavefunctions in the superconducting region from the BdG equation in Eq. (A7), i.e., the outgoing wavefunctions of the BP-NS junctions,

which is taken as

$$\begin{aligned}\Psi_{sh+}(x, y) &= \begin{pmatrix} e^{-i\beta} \\ e^{i\theta'_{sk+}} e^{-i\beta} \\ 1 \\ e^{i\theta'_{sk+}} \end{pmatrix} e^{i(k'_{sx+}x + k_y y)}, \\ \Psi_{se+}(x, y) &= \begin{pmatrix} e^{i\beta} \\ e^{i\theta_{sk+}} e^{i\beta} \\ 1 \\ e^{i\theta_{sk+}} \end{pmatrix} e^{i(k_{sx+}x + k_y y)},\end{aligned}\quad (\text{A15})$$

where

$$\begin{aligned}\beta &= \begin{cases} \arccos(E/\Delta) & \text{if } E < \Delta, \\ -i \operatorname{arccosh}(E/\Delta) & \text{if } E > \Delta, \end{cases} \\ e^{i\theta'_{sk+}} &= \frac{\left(\frac{E_g}{2} + \frac{\hbar^2(k'_{sx+})^2}{2m^*}\right)\tilde{\lambda}_x + i\hbar\tilde{v}_y k_y}{\sqrt{\left[\left(\frac{E_g}{2} + \frac{\hbar^2(k'_{sx+})^2}{2m^*}\right)\tilde{\lambda}_x\right]^2 + (\hbar\tilde{v}_y k_y)^2}}, \\ e^{i\theta_{sk+}} &= \frac{\left(\frac{E_g}{2} + \frac{\hbar^2 k_{sx+}^2}{2m^*}\right)\tilde{\lambda}_x + i\hbar\tilde{v}_y k_y}{\sqrt{\left[\left(\frac{E_g}{2} + \frac{\hbar^2 k_{sx+}^2}{2m^*}\right)\tilde{\lambda}_x\right]^2 + (\hbar\tilde{v}_y k_y)^2}}, \\ k'_{sx+} &= -\sqrt{\frac{2m^*}{\hbar} \left(\sqrt{(i\tau_1 - \tau_2)^2 - \left(k_y \frac{\tilde{v}_y}{\tilde{\lambda}_x}\right)^2} - \frac{E_g}{2\hbar} \right)}, \\ k_{sx+} &= \sqrt{\frac{2m^*}{\hbar} \left(\sqrt{(i\tau_1 + \tau_2)^2 - \left(k_y \frac{\tilde{v}_y}{\tilde{\lambda}_x}\right)^2} - \frac{E_g}{2\hbar} \right)}, \\ \tau_1 &= \frac{\Delta \sin \beta}{\hbar\tilde{\lambda}_x}, \quad \tau_2 = \frac{U + E_F}{\hbar\tilde{\lambda}_x}.\end{aligned}\quad (\text{A16})$$

APPENDIX B: ARS COEFFICIENTS OF THE BP-NS INTERFACE ORIENTATION ANGLE $\theta \neq 0^\circ$

In this Appendix, we provide the derivation process of ARs and NR coefficients under the BP-NS interface orientation angle $\theta \neq 0^\circ$.

After the coordinate transformation, the BdG Hamiltonian in Eq. (7) becomes

$$\tilde{H}'_{\text{BdG}} = \begin{pmatrix} \tilde{H}_+^{\text{eff}'} - \tilde{E}_F - \tilde{\mu}(\tilde{\mathbf{y}}') & \tilde{\Delta}(\tilde{\mathbf{y}}') \\ \tilde{\Delta}(\tilde{\mathbf{y}}')^* & -\tilde{H}_+^{\text{eff}'} + \tilde{E}_F + \tilde{\mu}(\tilde{\mathbf{y}}') \end{pmatrix}, \quad (\text{B1})$$

where

$$\tilde{H}_+^{\text{eff}'} = \left(\frac{\tilde{E}_g}{2} + \tilde{k}_x^2 \right) + \tilde{k}_y,$$

with $\tilde{k}_x = \tilde{k}_{y'} \sin \theta + \tilde{k}_{x'} \cos \theta$, $\tilde{k}_y = \tilde{k}_{y'} \cos \theta - \tilde{k}_{x'} \sin \theta$, and

$$\tilde{\mu}(\tilde{\mathbf{y}}') = \begin{cases} 0 & \tilde{y}' < 0 \\ \tilde{U} & \tilde{y}' > 0 \end{cases}, \quad \tilde{\Delta}(\tilde{\mathbf{y}}') = \begin{cases} 0 & \tilde{y}' < 0 \\ \tilde{\Delta} & \tilde{y}' > 0 \end{cases}. \quad (\text{B2})$$

The energy dispersion in the normal region ($\tilde{y}' < 0$) is

$$\begin{aligned}\tilde{E}_{e\pm} &= \pm \sqrt{\left(\frac{\tilde{E}_g}{2} + \tilde{k}_x^2 \right)^2 + \tilde{k}_y^2} - \tilde{E}_F, \\ \tilde{E}_{h\pm} &= \pm \sqrt{\left(\frac{\tilde{E}_g}{2} + \tilde{k}_x^2 \right)^2 + \tilde{k}_y^2} + \tilde{E}_F,\end{aligned}\quad (\text{B3})$$

The energy dispersion for quasiparticles in the superconducting ($\tilde{y}' > 0$) region is written as

$$\tilde{E}_s = \pm \sqrt{\left(\pm \sqrt{\left(\frac{\tilde{E}_g}{2} + \tilde{k}_x^2 \right)^2 + \tilde{k}_y^2} - \tilde{U} - \tilde{E}_F \right)^2 + \tilde{\Delta}^2}. \quad (\text{B4})$$

Assuming an electron from the conduction band \tilde{E}_{e+} enters the BP-NS interface, one can find that the modes for incident and reflected electrons (holes) in the normal region ($\tilde{y}' < 0$) can be given as follows:

$$\begin{aligned}\tilde{\Psi}_{e\pm'}(\tilde{y}', \tilde{x}') &= \begin{pmatrix} 1 \\ e^{i\theta_{k\pm'}} \\ 0 \\ 0 \end{pmatrix} e^{i(\tilde{k}_{y\pm'}\tilde{y}' + \tilde{k}_{x'}\tilde{x}')}, \\ \tilde{\Psi}_{h+'}(\tilde{y}', \tilde{x}') &= \begin{pmatrix} 0 \\ 0 \\ 1 \\ e^{i\theta'_{k+'}} \end{pmatrix} e^{i(\tilde{k}'_{y-}\tilde{y}' + \tilde{k}_{x'}\tilde{x}')}, \quad \text{if } \tilde{E} > \tilde{E}_F, \\ \tilde{\Psi}_{h-'}(\tilde{y}', \tilde{x}') &= \begin{pmatrix} 0 \\ 0 \\ 1 \\ e^{i\theta'_{k-'}} \end{pmatrix} e^{i(\tilde{k}'_{y+}\tilde{y}' + \tilde{k}_{x'}\tilde{x}')}, \quad \text{if } \tilde{E} < \tilde{E}_F,\end{aligned}\quad (\text{B5})$$

where

$$\begin{aligned}e^{i\theta_{k\pm'}} &= \frac{\left[\frac{\tilde{E}_g}{2} + (\tilde{k}_{y\pm'} \sin \theta + \tilde{k}_{x'} \cos \theta)^2 \right] + i(\tilde{k}_{y\pm'} \cos \theta - \tilde{k}_{x'} \sin \theta)}{\sqrt{\left[\frac{\tilde{E}_g}{2} + (\tilde{k}_{y\pm'} \sin \theta + \tilde{k}_{x'} \cos \theta)^2 \right]^2 + (\tilde{k}_{y\pm'} \cos \theta - \tilde{k}_{x'} \sin \theta)^2}}, \\ e^{i\theta'_{k\pm'}} &= \mp \frac{\left[\frac{\tilde{E}_g}{2} + (\tilde{k}'_{y\mp'} \sin \theta + \tilde{k}_{x'} \cos \theta)^2 \right] + i(\tilde{k}'_{y\mp'} \cos \theta - \tilde{k}_{x'} \sin \theta)}{\sqrt{\left[\frac{\tilde{E}_g}{2} + (\tilde{k}'_{y\mp'} \sin \theta + \tilde{k}_{x'} \cos \theta)^2 \right]^2 + (\tilde{k}'_{y\mp'} \cos \theta - \tilde{k}_{x'} \sin \theta)^2}}.\end{aligned}$$

The wavevectors for the incident electron and the reflected hole (electron) are (for simplicity, we set $\tilde{k}_{x'} = 0$)

$$\tilde{k}_{y\pm'} = \pm \sqrt{\frac{-p + \sqrt{p^2 + 4 \sin^4 \theta q}}{2 \sin^4 \theta}}, \quad \tilde{k}'_{y\pm'} = \pm \sqrt{\frac{-p + \sqrt{p^2 + 4 \sin^4 \theta q}}{2 \sin^4 \theta}}, \quad (\text{B6})$$

with $p = \tilde{E}_g \sin^2 \theta + \cos^2 \theta$, $q = (\tilde{E} + \tilde{E}_F)^2 - \left(\frac{\tilde{E}_g}{2}\right)^2$.

Following the above derivations, the wavefunctions $\tilde{\Psi}'_I(\tilde{y}', \tilde{x}')$ in the normal region (the $\tilde{y}' < 0$ region) can be written as

$$\tilde{\Psi}'_I(\tilde{y}', \tilde{x}') = \begin{cases} \tilde{\Psi}_{e+}' + r_N \tilde{\Psi}_{e-}' + r_A \tilde{\Psi}_{h-}' & \text{if } \tilde{E} < \tilde{E}_F, \\ \tilde{\Psi}_{e+}' + r_N \tilde{\Psi}_{e-}' + r_A \tilde{\Psi}_{h+}' & \text{if } \tilde{E} > \tilde{E}_F, \end{cases} \quad (\text{B7})$$

where r_N and r_A are the amplitudes of NR and ARs, respectively. The outgoing modes in the superconducting region

$$\begin{aligned} \tilde{\Psi}_{sh+}'(\tilde{y}', \tilde{x}') &= \begin{pmatrix} e^{-i\beta} \\ e^{i\tilde{\theta}'_{sk+}'} e^{-i\beta} \\ 1 \\ e^{i\tilde{\theta}'_{sk+}'} \end{pmatrix} e^{i(\tilde{k}'_{sy+}' \tilde{y}' + \tilde{k}'_{x'} \tilde{x}')}, \\ \tilde{\Psi}_{se+}'(\tilde{y}', \tilde{x}') &= \begin{pmatrix} e^{i\beta} \\ e^{i\tilde{\theta}'_{sk+}'} e^{i\beta} \\ 1 \\ e^{i\tilde{\theta}'_{sk+}'} \end{pmatrix} e^{i(\tilde{k}'_{sy+}' \tilde{y}' + \tilde{k}'_{x'} \tilde{x}')}, \end{aligned} \quad (\text{B8})$$

$$\beta = \begin{cases} \arccos(\tilde{E}/\tilde{\Delta}) & \text{if } \tilde{E} < \tilde{\Delta}, \\ -i \operatorname{arccosh}(\tilde{E}/\tilde{\Delta}) & \text{if } \tilde{E} > \tilde{\Delta}, \end{cases} \quad (\text{B9})$$

and the wavevectors in the superconducting region are

$$\begin{aligned} e^{i\tilde{\theta}'_{sk+}'} &= \frac{[\frac{\tilde{E}_g}{2} + (\tilde{k}'_{sy+}' \sin \theta + \tilde{k}'_{x'} \cos \theta)^2] + i(\tilde{k}'_{sy+}' \cos \theta - \tilde{k}'_{x'} \sin \theta)}{\sqrt{[\frac{\tilde{E}_g}{2} + (\tilde{k}'_{sy+}' \sin \theta + \tilde{k}'_{x'} \cos \theta)^2]^2 + (\tilde{k}'_{sy+}' \cos \theta - \tilde{k}'_{x'} \sin \theta)^2}}, \\ e^{i\tilde{\theta}_{sk+}} &= \frac{[\frac{\tilde{E}_g}{2} + (\tilde{k}_{sy+} \sin \theta + \tilde{k}_{x'} \cos \theta)^2] + i(\tilde{k}_{sy+} \cos \theta - \tilde{k}_{x'} \sin \theta)}{\sqrt{[\frac{\tilde{E}_g}{2} + (\tilde{k}_{sy+} \sin \theta + \tilde{k}_{x'} \cos \theta)^2]^2 + (\tilde{k}_{sy+} \cos \theta - \tilde{k}_{x'} \sin \theta)^2}}, \\ \tilde{k}'_{sy+} &= -\sqrt{\frac{-(\tilde{E}_g \sin^2 \theta + \cos^2 \theta) + \sqrt{(\tilde{E}_g \sin^2 \theta + \cos^2 \theta)^2 + 4 \sin^4 \theta [(\sqrt{\tilde{E}^2 - \tilde{\Delta}^2} - \tilde{U} - \tilde{E}_F)^2 - (\frac{\tilde{E}_g}{2})^2]}}{2 \sin^4 \theta}}, \\ \tilde{k}_{sy+} &= \sqrt{\frac{-(\tilde{E}_g \sin^2 \theta + \cos^2 \theta) + \sqrt{(\tilde{E}_g \sin^2 \theta + \cos^2 \theta)^2 + 4 \sin^4 \theta [(\sqrt{\tilde{E}^2 - \tilde{\Delta}^2} + \tilde{U} + \tilde{E}_F)^2 - (\frac{\tilde{E}_g}{2})^2]}}{2 \sin^4 \theta}}. \end{aligned} \quad (\text{B10})$$

When an electron is incident from the normal region, the wavefunctions $\tilde{\Psi}'_{II}(\tilde{y}', \tilde{x}')$ in the superconducting region ($\tilde{y}' > 0$) can be expressed as

$$\tilde{\Psi}'_{II}(\tilde{y}', \tilde{x}') = a \tilde{\Psi}_{sh+}' + b \tilde{\Psi}_{se+}', \quad (\text{B11})$$

where a and b are coefficients of the quasiparticle modes. Meanwhile, the matching condition of the wavefunctions at $\tilde{y}' = 0$ interface of the BP-NS junctions is given as

$$\tilde{\Psi}'_I(\tilde{y}', \tilde{x}')|_{\tilde{y}'=0^-} = \tilde{\Psi}'_{II}(\tilde{y}', \tilde{x}')|_{\tilde{y}'=0^+}. \quad (\text{B12})$$

For the case of $\tilde{E} < \tilde{E}_F$, we have

$$(\tilde{\Psi}_{e+}' + r_N \tilde{\Psi}_{e-}' + r_A \tilde{\Psi}_{h-}')|_{\tilde{y}'=0^-} = (a \tilde{\Psi}_{sh+}' + b \tilde{\Psi}_{se+}')|_{\tilde{y}'=0^+},$$

and the NR and the retro AR coefficients are

$$\begin{aligned} R_N &= \left| \frac{\langle \tilde{\Psi}_{e-}' | \tilde{J}_{y'} | \tilde{\Psi}_{e-}' \rangle}{\langle \tilde{\Psi}_{e+}' | \tilde{J}_{y'} | \tilde{\Psi}_{e+}' \rangle} \right| |r_N|^2, \\ R_A &= \left| \frac{\langle \tilde{\Psi}_{h-}' | \tilde{J}_{y'} | \tilde{\Psi}_{h-}' \rangle}{\langle \tilde{\Psi}_{e+}' | \tilde{J}_{y'} | \tilde{\Psi}_{e+}' \rangle} \right| |r_A|^2. \end{aligned} \quad (\text{B13})$$

On the other hand, for the case of $\tilde{E} > \tilde{E}_F$, we have

$$(\tilde{\Psi}_{e+}' + r_N \tilde{\Psi}_{e-}' + r_A \tilde{\Psi}_{h+}')|_{\tilde{y}'=0^-} = (a \tilde{\Psi}_{sh+}' + b \tilde{\Psi}_{se+}')|_{\tilde{y}'=0^+},$$

and the NR and the specular AR coefficients are

$$\begin{aligned} R_N &= \left| \frac{\langle \tilde{\Psi}_{e-}' | \tilde{J}_{y'} | \tilde{\Psi}_{e-}' \rangle}{\langle \tilde{\Psi}_{e+}' | \tilde{J}_{y'} | \tilde{\Psi}_{e+}' \rangle} \right| |r_N|^2, \\ R_A &= \left| \frac{\langle \tilde{\Psi}_{h+}' | \tilde{J}_{y'} | \tilde{\Psi}_{h+}' \rangle}{\langle \tilde{\Psi}_{e+}' | \tilde{J}_{y'} | \tilde{\Psi}_{e+}' \rangle} \right| |r_A|^2, \end{aligned} \quad (\text{B14})$$

with the expression of probability current being $\tilde{J}_{y'} = \tau_z \otimes \sigma_y$.

- [1] E. Moen and O. T. Valls, *Phys. Rev. B* **97**, 174506 (2018).
- [2] S. W. Jung, S. H. Ryu, W. J. Shin, Y. Sohn, M. Huh, R. J. Koch, C. Jozwiak, E. Rotenberg, A. Bostwick, and K. S. Kim, *Nat. Mater.* **19**, 277 (2020).
- [3] J. Linder and T. Yokoyama, *Phys. Rev. B* **89**, 020504(R) (2014).
- [4] R. Li, J.-F. Liu, and J. Wang, *Phys. Rev. Appl.* **19**, 024075 (2023).
- [5] Z. Wei, J. Tang, X. Li, Z. Chi, Y. Wang, Q. Wang, B. Han, N. Li, B. Huang, J. Li *et al.*, *Small Methods* **5**, 2100091 (2021).
- [6] Z. Wang, Q. Li, F. Besenbacher, and M. Dong, *Adv. Mater.* **28**, 10224 (2016).
- [7] Q. Zhang, Z. Chang, G. Xu, Z. Wang, Y. Zhang, Z. Q. Xu, S. Chen, Q. Bao, J. Z. Liu, Y. W. Mai *et al.*, *Adv. Funct. Mater.* **26**, 8707 (2016).
- [8] M. Akhtar, G. Anderson, R. Zhao, A. Alruqi, J. E. Mroczkowska, G. Sumanasekera, and J. B. Jasinski, *npj 2D Mater. Appl.* **1**, 5 (2017).
- [9] A. Carvalho, M. Wang, X. Zhu, A. S. Rodin, H. Su, and A. H. Castro Neto, *Nat. Rev. Mater.* **1**, 16061 (2016).
- [10] F. Xia, H. Wang, J. C. M. Hwang, A. H. C. Neto, and L. Yang, *Nat. Rev. Phys.* **1**, 306 (2019).
- [11] L. Li, Y. Yu, G. J. Ye, Q. Ge, X. Ou, H. Wu, D. Feng, X. H. Chen, and Y. Zhang, *Nat. Nanotechnol.* **9**, 372 (2014).
- [12] J. Kim, S. S. Baik, S. H. Ryu, Y. Sohn, S. Park, B. G. Park, J. Denlinger, Y. Yi, H. J. Choi, and K. S. Kim, *Science* **349**, 723 (2015).
- [13] X. Wang, A. M. Jones, K. L. Seyler, V. Tran, Y. Jia, H. Zhao, H. Wang, L. Yang, X. Xu, and F. Xia, *Nat. Nanotechnol.* **10**, 517 (2015).
- [14] V. Tran, R. Soklaski, Y. Liang, and L. Yang, *Phys. Rev. B* **89**, 235319 (2014).
- [15] Z. Luo, J. Maassen, Y. Deng, Y. Du, R. P. Garrelts, M. S. Lundstrom, P. D. Ye, and X. Xu, *Nat. Commun.* **6**, 8572 (2015).
- [16] R. Fei, A. Faghaninia, R. Soklaski, J.-A. Yan, C. Lo, and L. Yang, *Nano Lett.* **14**, 6393 (2014).
- [17] J. Qiao, X. Kong, Z.-X. Hu, F. Yang, and W. Ji, *Nat. Commun.* **5**, 4475 (2014).
- [18] G. Long, D. Maryenko, S. Pezzini, S. Xu, Z. Wu, T. Han, J. Lin, C. Cheng, Y. Cai, U. Zeitler, and N. Wang, *Phys. Rev. B* **96**, 155448 (2017).
- [19] Y. W. Choi and H. J. Choi, *2D Mater.* **8**, 035024 (2021).
- [20] Z. Li, T. Cao, M. Wu, and S. G. Louie, *Nano Lett.* **17**, 2280 (2017).
- [21] S.-G. Chen, B.-Y. Zhang, Z.-W. Yang, and W.-J. Gong, *Phys. Chem. Chem. Phys.* **25**, 23836 (2023).
- [22] Y. Betancur-Ocampo, F. Leyvraz, and T. Stegmann, *Nano Lett.* **19**, 7760 (2019).
- [23] A. F. Andreev, *Zh. Eksp. Teor. Fiz.* **46**, 1823 (1964).
- [24] C. W. J. Beenakker, *Phys. Rev. Lett.* **97**, 067007 (2006).
- [25] P. Ram, D. Beckmann, R. Danneau, and W. Belzig, *Phys. Rev. B* **108**, 184510 (2023).
- [26] W.-T. Lu and Q.-F. Sun, *Phys. Rev. B* **108**, 195425 (2023).
- [27] L. Majidi and R. Asgari, *Phys. Rev. B* **93**, 195404 (2016).
- [28] Q. Cheng and Q.-F. Sun, *Phys. Rev. B* **103**, 144518 (2021).
- [29] S.-G. Cheng, Y. Xing, J. Wang, and Q.-F. Sun, *Phys. Rev. Lett.* **103**, 167003 (2009).
- [30] S.-G. Cheng, H. Zhang, and Q.-F. Sun, *Phys. Rev. B* **83**, 235403 (2011).
- [31] Q. Zhang, D. Fu, B. Wang, R. Zhang, and D.-Y. Xing, *Phys. Rev. Lett.* **101**, 047005 (2008).
- [32] X. Zhou, *Phys. Rev. B* **102**, 045132 (2020).
- [33] Y. Deng, Z. Luo, N. J. Conrad, H. Liu, Y. Gong, S. Najmaei, P. M. Ajayan, J. Lou, X. Xu, and P. D. Ye, *ACS Nano* **8**, 8292 (2014).
- [34] A. Avsar, I. J. Vera-Marun, J. Y. Tan, K. Watanabe, T. Taniguchi, A. H. Castro Neto, and B. Özyilmaz, *ACS Nano* **9**, 4138 (2015).
- [35] P. J. Jeon, Y. T. Lee, J. Y. Lim, J. S. Kim, D. K. Hwang, and S. Im, *Nano Lett.* **16**, 1293 (2016).
- [36] J. E. Padilha, A. Fazzio, and A. J. R. da Silva, *Phys. Rev. Lett.* **114**, 066803 (2015).
- [37] K. J. Lamas-Martínez, J. A. Briones-Torres, S. Molina-Valdovinos, and I. Rodríguez-Vargas, *Phys. Rev. B* **107**, 245427 (2023).
- [38] J. Linder and T. Yokoyama, *Phys. Rev. B* **95**, 144515 (2017).
- [39] R. Li, L. Chen, J. F. Liu, and J. Wang, *Sci. Rep.* **12**, 6079 (2022).
- [40] M. Alidoust, M. Willatzen, and A.-P. Jauho, *Phys. Rev. B* **98**, 184505 (2018).
- [41] M. Alidoust, M. Willatzen, and A.-P. Jauho, *Phys. Rev. B* **99**, 125417 (2019).
- [42] W. Chen, Z.-Y. Xu, W.-H. Tian, Y.-Y. Lv, M. Yu, X.-J. Zhou, X.-C. Tu, J.-B. Wu, J. Li, S.-L. Li *et al.*, *Supercond. Sci. Technol.* **32**, 115005 (2019).
- [43] Z.-Y. Xu, W. Chen, J.-W. Huang, W.-H. Tian, S.-X. Chen, W.-C. Yue, T.-Y. Chi, Y.-Y. Lyu, H.-C. Sun, Y.-L. Wang *et al.*, *Appl. Phys. Lett.* **119**, 072601 (2021).
- [44] F. Telesio, M. Carrega, G. Cappelli, A. Iorio, A. Crippa, E. Strambini, F. Giazotto, M. Serrano-Ruiz, M. Peruzzini, and S. Heun, *ACS Nano* **16**, 3538 (2022).
- [45] T. Oka and H. Aoki, *Phys. Rev. B* **79**, 081406(R) (2009).
- [46] H. L. Calvo, H. M. Pastawski, S. Roche, and L. E. F. F. Torres, *Appl. Phys. Lett.* **98**, 232103 (2011).
- [47] T. Kitagawa, T. Oka, A. Brataas, L. Fu, and E. Demler, *Phys. Rev. B* **84**, 235108 (2011).
- [48] J. Cayssol, B. Dóra, F. Simon, and R. Moessner, *Phys. Status Solidi RRL* **7**, 101 (2013).
- [49] A. López, A. Scholz, B. Santos, and J. Schliemann, *Phys. Rev. B* **91**, 125105 (2015).
- [50] M. Ezawa, *Phys. Rev. Lett.* **110**, 026603 (2013).
- [51] Y. Xu and X. Zhou, *Resul. Phys.* **27**, 104523 (2021).
- [52] A. Iurov, L. Zhemchuzhna, G. Gumbs, and D. Huang, *J. Appl. Phys.* **122**, 124301 (2017).
- [53] S.-H. Zhou, C.-H. Bao, B.-S. Fan, H. Zhou, Q.-X. Gao, H.-Y. Zhong, T.-Y. Lin, H. Liu, P. Yu, P. Tang *et al.*, *Nature (London)* **614**, 75 (2023).
- [54] S. S. Baik, K. S. Kim, Y. Yi, and H. J. Choi, *Nano Lett.* **15**, 7788 (2015).
- [55] H. Doh and H. J. Choi, *2D Mater.* **4**, 025071 (2017).
- [56] X. Zhou, Y. Xu, and G. Jin, *Phys. Rev. B* **92**, 235436 (2015).
- [57] P. G. De Gennes, *Superconductivity of Metals and Alloys* (Benjamin, New York, 1966).
- [58] S.-H. Zhang and W. Yang, *Phys. Rev. B* **97**, 235440 (2018).
- [59] X. Zhou, *Phys. Rev. B* **100**, 195139 (2019).
- [60] G. E. Blonder, M. Tinkham, and T. M. Klapwijk, *Phys. Rev. B* **25**, 4515 (1982).